9. X.X. Yang, B. Gong, G. Tan, and Z. Lu, Reconfigurable patch antennas with four-polarization states agility using dual feed port, Prog Electromagn Res B 54 (2013), 285–301.
10. Y. Cao, S.W. Cheung, X.L. Sun, and T.I. Yuk, Frequency-reconfigurable monopole antenna with wide tuning range for cognitive radio, Microwave Opt Technol Lett 56 (2014), 145–152.
11. D.-A. Lee and Y.J. Sung, Reconfigurable PIFA/LOOP antenna for mobile handset applications, Microwave Opt Technol Lett 56 (2014), 2034–2037.
12. S.W. Lee and Y.J. Sung, A frequency reconfigurable planar inverted-F antenna for WWAN mobile handset applications, Microwave Opt Technol Lett 56 (2014), 2888–2893.
13. S. Kang and C.W. Jung, Reconfigurable beam steering using U-slot patch antenna with high gain and low SAR for wireless headset applications, Microwave Opt Technol Lett 57 (2015), 542–547.
14. M.S. Alam and A.M. Abbosh, Beam-steerable planar antenna using circular disc and four PIN-controlled tapered stubs for WiMAX and WLAN applications, IEEE Antennas Wireless propag Lett 15 (2016), 980–983.
15. J. Kumar, F.A. Talukdar, and B. Basu, Frequency reconfigurable E-shaped patch antenna for medical applications, Microwave Opt Technol Lett 58 (2016), 2214–2217.
16. N. Kishore, A. Prakash, and V.S. Tripathi, A multiband microstrip patch antenna with defected ground structure for ITS applications, Microwave Opt Technol Lett 58 (2016), 2814–2818.
17. C. Laxey, L. Dussopt, J.-L. Le Sonn, and J.-M. Laheurte, Dual-frequency operation of CPW-fed antenna controlled by PIN diodes, Electron Lett 36 (2000), 2.3.
18. L. Gauffret, J. Laherute, and A. Papiernik, Study of various shapes of the coupling slot in CPW-fed microstrip antennas, IEEE Trans Antennas Propag 45 (1997), 642–647.
19. ANSYS, ANSYS Academic Research, Release v15.0.

COMPACT UWB MIMO ANTENNA WITH PATTERN DIVERSITY AND BAND REJECTION CHARACTERISTICS

Ahmed A. Ibrahim,[1,2] Jan Machac,[3] and Raed M. Shubair[4,5]
[1] Faculty of Engineering, Minia University, Minya, UAE; Corresponding author: ahmedabdel_monem@mu.edu.eg
[2] Institute of Micro- and Sensor Systems, University of Magdeburg, Magdeburg, Germany
[3] Department of Electromagnetic Field, Czech Technical University in Prague, Technicka 2, Prague 166 27, Czech Republic
[4] Electrical and Computer Engineering Department, Khalifa University, UAE
[5] Research Laboratory of Electronics, Massachetts Institute of Technology, USA

Received 11 November 2016

ABSTRACT: *This article presents a compact size asymmetric CPW strip-fed UWB two-element MIMO antenna, with notched-band behavior. The single-antenna element of the MIMO configuration is composed of a semi-elliptical patch radiator with asymmetric ground plane. The notched-band behavior of the proposed antenna is achieved by inserting a simple folded stub to the patch radiator. This stub achieves the desired single stop-band from 3.3 to 3.9 GHz for WIMAX. The two-antenna elements are placed orthogonally to achieve pattern diversity which leads to an improved MIMO system performance and enhances the isolation between elements without using any decoupling structures. The antenna has dimensions of 50 × 28 mm^2. The edge-to-edge distance between antenna elements is 0.15λ0 at 3 GHz. The proposed antenna is designed, simulated, fabricated, and tested. Results show that the two-antenna elements operate at frequencies ranging from 2.8 to 11.5 GHz with return loss lower than −10 dB and insertion loss lower than −18 dB. The performance of the MIMO antenna diversity characteristics were verified through the calculation of the standard parameters and show the antenna suitability for MIMO systems.* © 2017 Wiley Periodicals, Inc.
Microwave Opt Technol Lett 59:1460–1464, 2017; View this article online at wileyonlinelibrary.com. DOI 10.1002/mop.30564

Key words: *MIMO antenna; UWB antenna; pattern diversity*

1. INTRODUCTION

UWB Communications run at frequency band from 3.1 to 10.6 GHz [1]. The UWB technology achieves the demand of low power level and high data rates [2]. Antennas play an important role in the UWB system to fulfill such demand. Features of planar antennas such as low profile, compact size, easy of fabrication, and low cost make them favorable in the design of UWB systems [3,4].

Utilization of MIMO systems is considered as one of the best ways to improve channel capacity and reduce multipath fading [5–7]. In MIMO systems, multiple and uncorrelated antenna elements are used to transmit and receive signals. Therefore, MIMO systems with pattern diversity use antenna elements with different radiation patterns to reduce channel fading and enhance transmission quality [8].

In portable devices, the design of MIMO antennas is considered as a challenging task as the antenna elements have to be located close to each other in a small area. The spacing between these two antenna elements must be, however, at least half a wavelength, at the lowest operating frequency of the UWB band to achieve an isolation coefficient better than −15 dB. This isolation is required to overcome multipath fading problems in MIMO systems [7,9]. Many approaches have been used to achieve high isolation between antenna elements, while keeping the electrical size of the antenna small, by utilizing decoupling structures as DGS [5]. Another approach was presented in Ref. [7], where the MIMO antenna elements are to assure the insertion loss lower than −15 dB decoupled by two stubs separated by a slot in ground metal layer.

The main advantage of CPW fed antenna [10] is its simplicity for integration with microwave circuits. However, the CPW-fed antenna occupies a large area. The asymmetric coplanar strip (ACS) used instead of CPW reduces the overall antenna size to about one half of the CPW-fed antennas [11].

This article presents a two-element UWB MIMO antenna with notched-band response and with a compact size. The antenna consists of two semi-elliptical radiating elements fed by ACS to achieve the bandwidth allocated for UWB applications which ranges from 3.1 to 10.6 GHz, with more than −18 dB measured insertion loss through the entire UWB frequency range, without using decoupling structures between the elements. Simulations done in the CST Microwave Studio verified the behavior of the designed UWB MIMO antenna and are fully in conformity with measurements of the fabricated antenna specimen.

2. UWB MIMO ANTENNA CONFIGURATION

Figure 1 shows the layout of presented antenna designed on FR4 substrate 1.6 mm in thickness and with permittivity equal to 4.4. To achieve 50 Ω characteristic impedance of the feeding ACS line, the ACS structure with a single strip 3 mm in width and gap distance 0.3 mm is used. The two-antenna elements are composed of semi-elliptical patch radiator with simple folded stub to achieve notched-band features. The two antenna elements are put orthogonally, so one element is horizontally excited, and the other is vertically excited, to achieve the desired diversity behavior. The ACS ground has a small curvature that

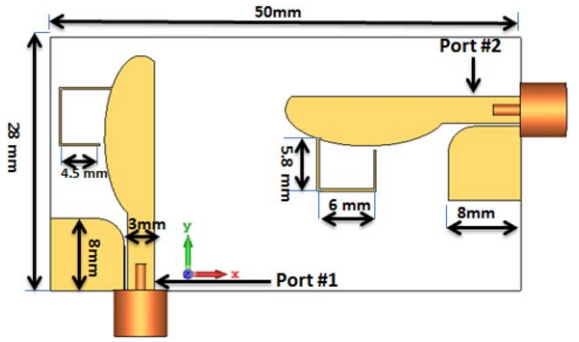

Figure 1 Configuration of the proposed UWB MIMO antenna. [Color figure can be viewed at wileyonlinelibrary.com]

enhances the impedance bandwidth of the antenna. Antenna layout dimensions are optimized to achieve the maximum bandwidth. At the same time, the proposed layout reduces antenna size to area of rectangle 50 × 28 mm^2. The distance between the two-antenna elements has been minimized to 15 mm; that is, 0.15 λ at 3 GHz. Figure 2 shows the photograph of the fabricated antenna.

3. RESULTS AND DISCUSSION

The UWB MIMO antenna is designed optimized, verified using CST microwave studio, fabricated, and measured.

3.1. S-Parameters of the Proposed UWB MIMO Antenna

Figure 3 shows simulated and measured return and insertion loss of the proposed UWB MIMO antenna. Similar results can be obtained when the antenna is fed at Port 2. R&S vector network analyzer ZVA40 was used. Simulation results illustrate that the proposed antenna operates at wide frequency band, ranging from 2.8 to 11.5 GHz, for which the return loss is lower than −10 dB except for the notched frequency band from 3.3 to 3.9 GHz. On the other hand, within that operating band, the isolation coupling is better than −15 dB at frequency bands from 4 to 5 GHz and from 7.5 to 9 GHz, and goes lower than −20 dB at other frequencies. Measurement indicates that the antenna operates in a frequency band ranging from 2.5 to 11 GHz, with return loss lower than −10 dB, coupling isolation better than −16 dB within the applicable frequency band. Measured S parameters do not fit precisely simulation results. This is due to the not perfectly soldered connectors and the tolerances of fabrication process. The overall character of measured and simulated data is however satisfactory.

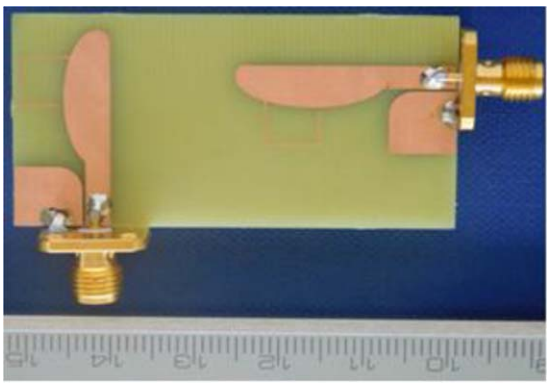

Figure 2 Photograph of the fabricated UWB MIMO antenna. [Color figure can be viewed at wileyonlinelibrary.com]

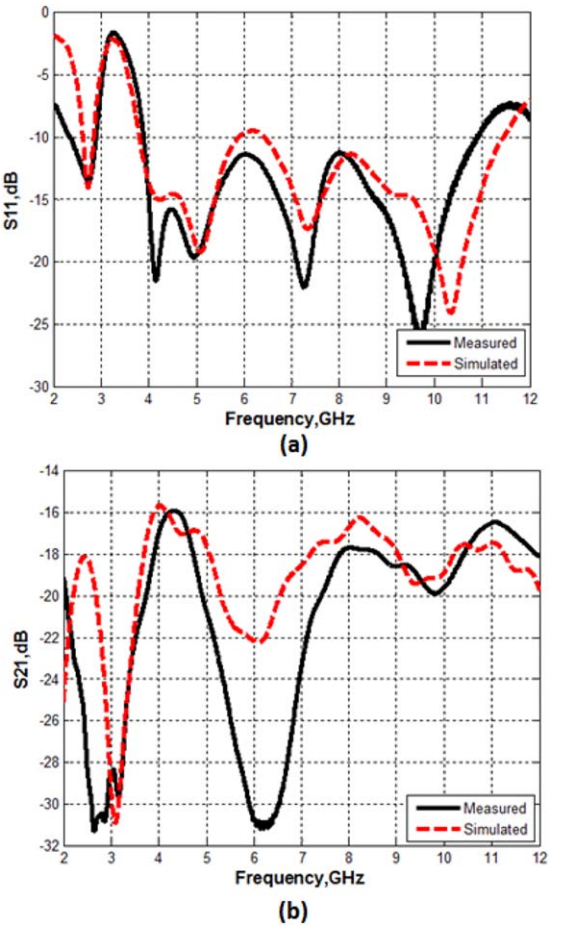

Figure 3 Measured and simulated S-parameters of the proposed UWB MIMO antenna: (a) S11; (b) S21. [Color figure can be viewed at wileyonlinelibrary.com]

3.2. Far-Field Radiation Patterns

Figure 4 shows 3D radiation patterns of the presented antenna calculated by the CST Microwave Studio at different frequencies using excitation in one port and at the same time the other port is matched with 50 Ω load. It is clear that the radiation pattern of Antenna 1 and Antenna 2 are mutually orthogonal, which indicates a good polarization and pattern diversity. The normalized directive gain in both (x–z) at $\varphi = 0°$,(x–y) at $\theta = 90°$ planes of the proposed UWB MIMO antenna at 3.5 GHz (the center of the notched band) and 10 GHz are shown in Figures 5 and 6. The antenna is measured in an anechoic chamber using the NSI 800F-30 system. The measurement was obtained assuming the excitation at Port 1, while Port 2 is matched with 50 Ω load and vice versa. Because the two antennas are orthogonally placed, it can be seen that the x–z planes of Port 1and Port 2 are rotated by 90°, and that the x–y plane of Port 1 is almost similar to the x–y plane of Port 2. This entails that the proposed antenna is suitable for diversity systems. The antenna radiation is almost omnidirectional. However, there is a small mess in the radiation patterns which is due to the asymmetric ground plane of the ACS feeding structure. Finally, we can observe that there is reasonable agreement between the simulated and measured radiation patterns in both planes.

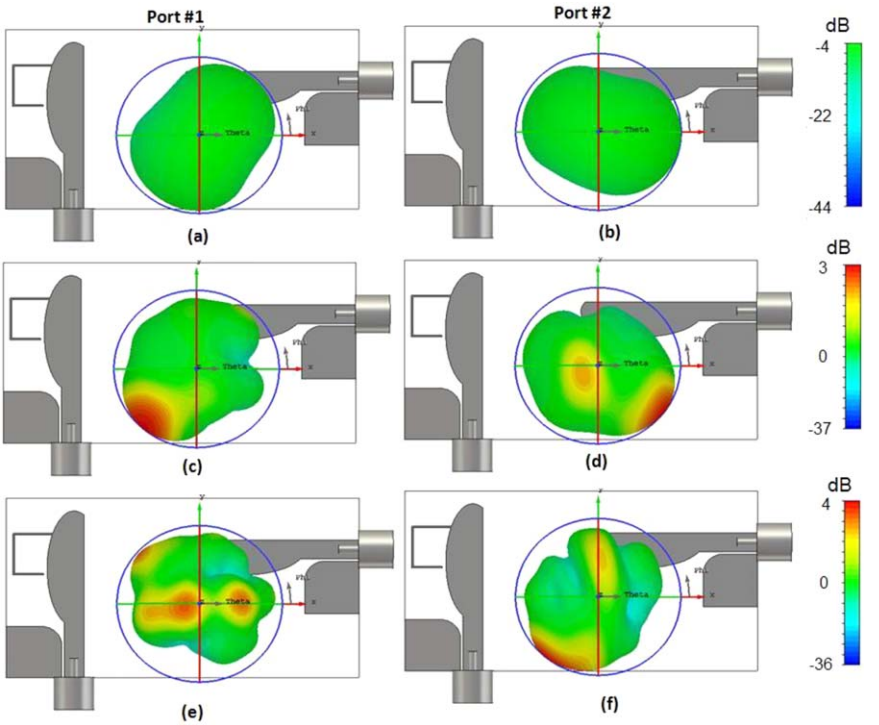

Figure 4 Simulated 3D radiation patterns of the proposed UWB MIMO antenna (a) at Port 1 at 3.5 GHz, (b) at Port 2 at 3.5 GHz, (c) at Port 1at 6 GHz, (d) at Port 2 at 6 GHz, (e) at Port 1 at 10 GHz, and (f) at Port 2 at 10 GHz. [Color figure can be viewed at wileyonlinelibrary.com]

3.3. Envelope Correlation Coefficient and Diversity Gain

The diversity capability of the proposed MIMO antenna is specified by envelope correlation coefficient (ECC), diversity gain (DG), and channel capacity loss (CCL).

The ECC is used to measure the correlation between the two-antenna elements. This correlation coefficient should be of a small value, to indicate higher diversity between the two-MIMO-antenna elements [12]. In the case of uniform multipath environment, ECC is given by [12]

$$\mathrm{ECC}=\frac{\left|S_{11}^{*}S_{12}+S_{21}^{*}S_{22}\right|^{2}}{\left(1-\left(\left|S_{11}\right|^{2}+\left|S_{21}\right|^{2}\right)\right)\left(1-\left(\left|S_{22}\right|^{2}+\left|S_{12}\right|^{2}\right)\right)}. \quad (1)$$

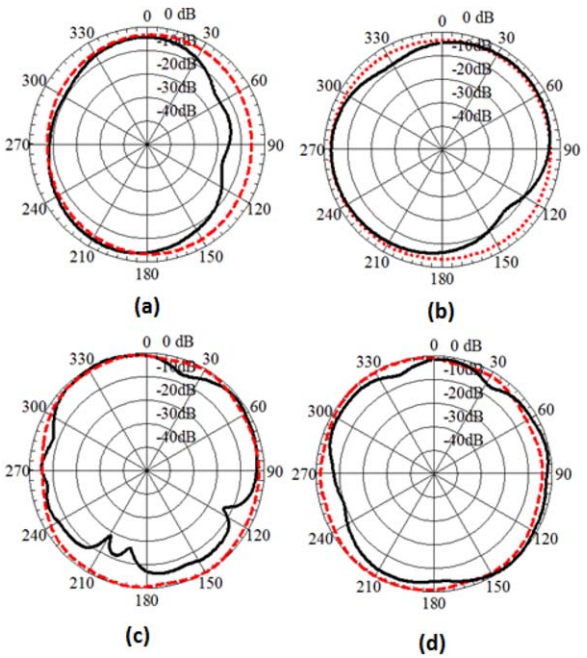

Figure 5 Measured black (solid) and simulated red (dashed) radiation patterns at Port 1 when Port 2 is matched: (a) *x–z* plane at 3.5 GHz, (b) *x–y* plane at 3.5 GHz, (c) *x–z* plane at 10 GHz, and (d) *x–y* plane at 10 GHz. [Color figure can be viewed at wileyonlinelibrary.com]

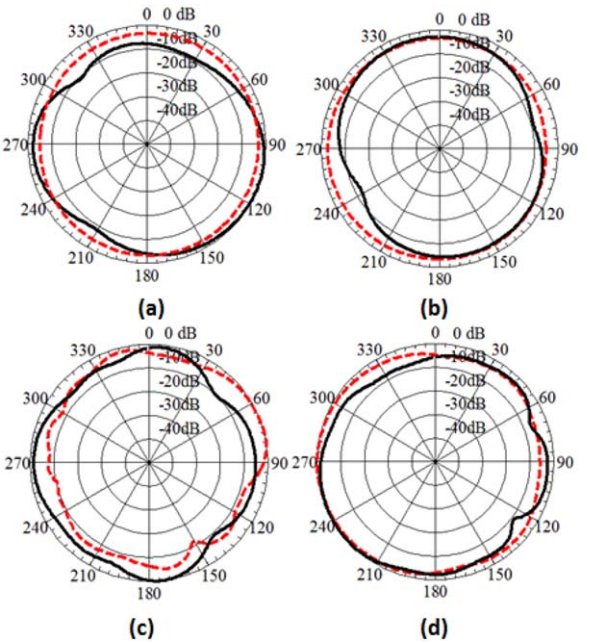

Figure 6 Measured black (solid) and simulated red (dashed) radiation patterns at Port 2 when Port 1 is matched: (a) *x–z* plane at 3.5 GHz, (b) *x–y* plane at 3.5 GHz, (c) *x–z* plane at 10 GHz, and (d) *x–y* plane at 10 GHz. [Color figure can be viewed at wileyonlinelibrary.com]

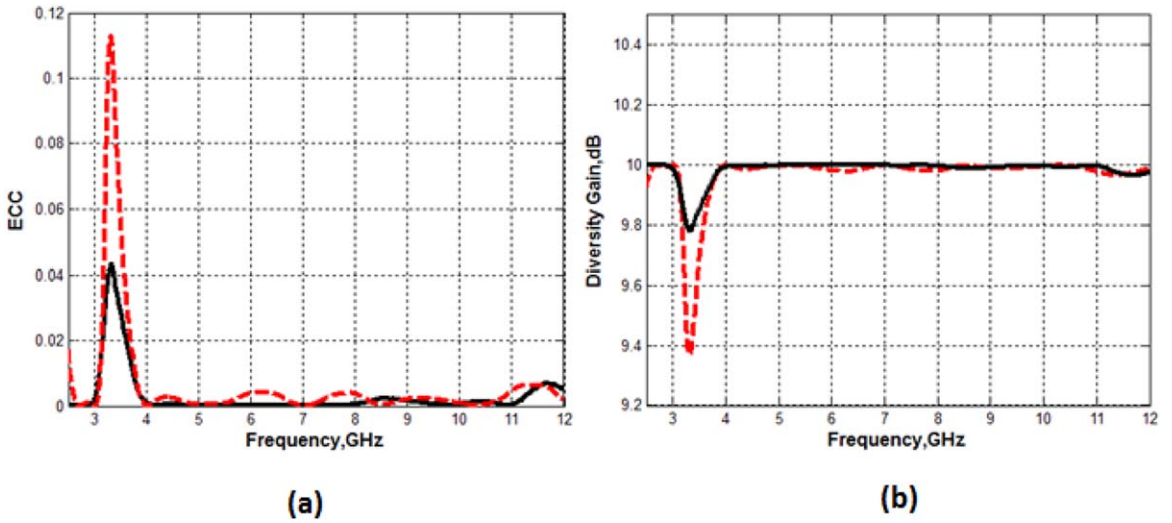

Figure 7 Measured black (solid) and simulated red (dashed) results of the proposed UWB MIMO antenna: (a) envelope correlation coefficient and (b) diversity gain. [Color figure can be viewed at wileyonlinelibrary.com]

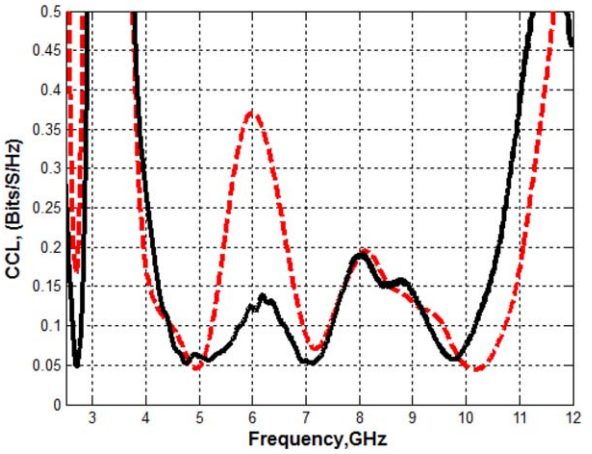

Figure 8 Measured black (solid) and simulated red (dashed) channel capacity loss of the proposed UWB MIMO antenna. [Color figure can be viewed at wileyonlinelibrary.com]

It is desirable to have ECC < 0.5 [13]. The simulated ECC is plotted in Figure 7(a). ECC of the MIMO antenna has value lower than 0.0003 within the operating frequency band, except the range from 3 to 3.8 GHz, where ECC increases to 0.12 (the frequency band of the notch). It can be concluded that the correlation between the two antennas elements is very low, and hence the diversity features of the proposed MIMO are strong.

The DG is coupled with ECC through [5]

$$\mathrm{DG} = 10 \times \sqrt{1 - |\mathrm{ECC}|}. \tag{2}$$

The DG of the designed antenna is plotted in Figure 7(b). Its value is around 10 dB within the whole operating frequency band, except for the notched band where it is reduced to 9 dB.

3.4. Channel Capacity Loss

The correlation between elements in MIMO systems produces CCL, which is calculated using [14]

$$\mathrm{CCL} = -\log_2 \det(\psi^R), \tag{3}$$

$$\psi^R = \begin{bmatrix} \rho_{11} & \rho_{12} \\ \rho_{21} & \rho_{22} \end{bmatrix}$$
$$\text{where } \rho_{ii} = \left(|S_{ii}|^2 + |S_{ij}|^2\right) \tag{4}$$
$$\rho_{ij} = -\left(S_{ii}^* S_{ij} + S_{ji}^* S_{ij}\right) \quad \text{for } i,j = 1 \text{ or } 2.$$

Typically, it is desirable to have CCL < 0.4 bits/s/Hz [15]. The simulated and measured results of CCL are plotted in Figure 8, where it can be observed that CCL is lower than 0.4 bits/s/Hz, from 4 to 11 GHz. CCL naturally increases in the notched frequency band from 3 to 3.8 GHz.

TABLE 1 Comparison Between the Proposed Antenna and Most Recent Published Work

Ref.	Antenna Size (cm^2)	ε_r/Thickness (mm)	BW (GHz)	Number of Radiators	Isolation (dB)
This Work	5 × 2.8	4.4/1.6	8.7	2	−18
[2]	3.2 × 3.2	4.4/0.8	7.5	2	−15
[6]	5.5 × 2.6	4.4/1.6	9.2	2	−20
[9]	4 × 3	4.4/0.8	7.5	2	−15
[7]	4 × 2.6	3.5/0.8	7.5	2	−15

Figures 7 and 8 confirm that the designed UWB MIMO antenna assures a good MIMO performance. Table 1 compares the designed antenna with the most recently published antennas.

4. CONCLUSION

UWB two-elements MIMO antenna with notched-band features was investigated. By placing the antenna elements orthogonally, good pattern diversity has been achieved and the performance of MIMO system has been improved. Also the isolation between elements has been improved without using any decoupling structures. The stop-band created by the resonant stub prevents the interference with WIMAX system. The designed antenna was fabricated, and measured parameters agree well with results of simulations. This verifies the suitability of the presented antenna for particular UWB MIMO applications.

REFERENCES

1. Federal Communications Commission, "Federal communications commission revision of Part 15 of the commission's rules regarding ultra-wideband transmission system from 3.1 to 10.6 GHz," FCC, Washington, DC, ET-Docket, 98–153, 2002.
2. J. Ren, W. Hu, Y. Yin, and R. Fan, Compact printed MIMO antenna for UWB applications, IEEE Antennas Wireless Propag Lett 13 (2014), 1517–1520.
3. A. Abdelreheem and M. Abdalla, Compact curved half circular disc-monopole UWB antenna, Int J Microwave Wireless Technol (2015), 1–8.
4. M.A. Abdalla, A.A. Ibrahim, and A. Boutejdar, Resonator switching for UWB antenna in wireless applications, IET Microwaves Antennas Propag 9 (2015), 1468–1477.
5. M.A. Abdalla and A.A. Ibrahim, Compact and closely spaced metamaterial MIMO antenna with high isolation for wireless applications, IEEE Wireless Propag Lett 12 (2013), 1452–1455.
6. A. Toktas Ali Akdagli, Compact multiple-input multiple-output antenna with low correlation for ultra-wide-band applications, IET Microwaves Antennas Propag 9 (2015).
7. L. Liu, S.W. Cheung, and T.I. Yuk, Compact MIMO antenna for portable devices in UWB applications, IEEE Trans Antennas Propag 61 (2013), 4257–4264. Aug.
8. K.P. Wei, Z.J. Zhang, W.H. Chen, and Z.H. Feng, A novel hybrid-fed patch antenna with pattern diversity, IEEE Antennas Wireless Propag Lett 9 (2010), 562–565.
9. T.-C. Tang, and K.-H. Lin, An ultrawideband MIMO antenna with dual band-notched function, IEEE Antennas Wireless Propag Lett 13 (2014), 1076–1079.
10. M.-N. Moghadasi, R.A. Sadeghzadeh, T. Sedghi, T. Aribi, and B.S. Virdee, UWB CPW-fed fractal patch antenna with band-notched function employing folded T-shaped element, IEEE Antennas Wireless Propag Lett 12 (2013), 507–507.
11. X. Li, X.W. Shi, W. Hu, P. Fei, and J.F. Yu, Compact triband ACS-fed monopole antenna employing open-ended slots for wireless communication, IEEE Antennas Wireless Propag Lett 12 (2013), 104–107.
12. S. Blanch, J. Romeu, and I. Corbella, Exact representation of antenna system diversity performance from input parameter description, Electron Lett 39 (2003),
13. C.X. Mao and Q.X. Chu, Compact co-radiator UWB-MIMO antenna with dual polarization, IEEE Trans Antennas Propag 62 (2014), 4474–4480.
14. H. Shin and J.H. Lee, Capacity of multiple-antenna fading channels: Spatial fading correlation, double scattering, and keyhole, IEEE Trans Inform Theory 49 (2003), 2636–2647.
15. Y.K. Choukiker, S.K. Sharma, and S.K. Behera, Hybrid fractal shape planar monopole antenna covering multiband wireless communications with MIMO implementation for handheld mobile devices, IEEE Trans Antennas Propag 62 (2014), 1483–1488.

NOVEL TRI-BAND BANDPASS FILTER WITH ONE HIGH SELECTIVE TUNABLE PASSBAND

Xuekun Du, Chang Jiang You, Jingye Cai, Zhaosheng He, Mengkui Shen, and Yuting Jiang
University of Electronic Science and Technology of China, 611731 Chengdu, China; Corresponding author: cjyou@uestc.edu.cn

Received 22 November 2016

ABSTRACT: *A novel tri-band bandpass filter (BPF) with one high selective tunable passband is presented in this letter. The tri-band bandpass-filtering response is implemented by using a pair of varactor-loaded square split rings, an open stub and a one-end shorted closed-loop ring. By loading an open stub at the central position of the proposed resonator, the odd-mode resonance can be split into two modes for generating high selective tunable passband. The simulated and measured results are in good agreement. The measured results indicate that the first-passband is fixed at 760 MHz with a 3-dB bandwidth of 40 MHz, and the third-passband is fixed at 2300 ± 35MHz with 4.7–6.2% 3-dB fractional bandwidth. The measured second-passband is with a 3-dB constant bandwidth of 95 ± 10 MHz and its centre frequency has 360 MHz tunable range.* © 2017 Wiley Periodicals, Inc. Microwave Opt Technol Lett 59:1464–1468, 2017; View this article online at wileyonlinelibrary.com. DOI 10.1002/mop.30562

Key words: *high selectivity; source-load coupling; tri-band bandpass filter; tunable filter; varactor-loaded square split ring resonator*

1. INTRODUCTION

Tri-band bandpass filter (BPF) with good performance is one of the essential tunable devices for multi-band communication systems due to its excellent features, such as compact size, low system complexity, and low fabrication cost. In recent years, stub loaded resonators (SLRs), stepped-impedance resonators (SIRs), square ring loaded resonators (SRLRs) and stub loaded open-loop resonators were proven to realize the tri-band BPF design [1–8]. The method presented in [1,2] used multi-stubs to generate different odd/even- modes in order to form the desired passbands, but it was inconvenient for loading varactors due to the difficulty of tuning odd/even-mode resonances synchronously. The method in [3,4] indicated that the stub loaded SIRs can obtain multi-band behaviours and tuning the loaded stubs can change the centre frequencies of different bands. However, it is not easy to load varactors on the resonators employed in [3,4] due to their compact internal-structure. The SRLRs used in [5,6] had flexibility for high-order tri-band BPF design by tuning their geometric parameters. However, this structure has disadvantages for loading varactors due to its closed structure. Even the varactors were loaded, the passband selectivity was not high [7]. The stub loaded open-loop resonator presented in [8] was employed to realize a tri-band response by loading three open stubs and this structure was easy to load varactors, but the resonant mode could not be controlled independently under the condition of loading varactors.

In this letter, a novel tri-band BPF structure is presented to solve the difficulty of loading varactors and the poor selectivity of passband as discussed above. The frequency selectivity can be improved by introducing TZs located close to either sides of the desired passband. And the desired TZs can be realized by loading an open stub between the two varactor-loaded square split rings. The proposed resonator is composed of a pair of varactor-loaded square split rings, an open stub and a one-end